SAND2015-6759J

Role of Corners in Fracture of Polymeric Adhesives

Mark J. Stevens

Sandia National Laboratories, Center for Integrated Nanotechnologies, Albuquerque, NM 87185-1315

(Dated: August 5, 2015)

Abstract

Tensile simulations with open ends between two solid adherends have been performed for coarse-grained, highly crosslinked polymer networks modeling epoxy systems. The open boundary and the presence of corners dramatically alters the fracture behavior. In contrast to systems with periodic boundaries, the failure strain decreases with increasing system size. This decrease greatly reduces the difference between simulation and experiment. In the open geometry, the sides of the polymer network neck inward forming wedge shaped corners where the crack initiation occurs. The deformation of the open ends is constrained by the minimal paths in the network connecting the two adherends. The crack initiation in the corners is consistent with a diverging stress in the corners according to fracture mechanics. The local stress in the corners becomes large well before failure, but in the direction parallel to the interface due to the deformation of the corners into the wedge shape.

The mechanics of polymer adhesives is intrinsically multiscale involving the bonding of one material to another at the molecular scale and the stresses applied at the macro scale [1–3]. Polymeric adhesives are the preferred bonding method for many applications, because they produce excellent interfacial bonds and dissipate stresses on larger scales. In particular, epoxies are highly crosslinked polymer networks preferred in structural applications. Understanding the molecular mechanisms of fracture in such systems is a complex challenge of connecting molecular structure over multiple length scales with mechanical behavior. Linear elasticity theory gives a connection between the local stress at a corner between the adhesive and the adherend and the thickness of the adhesive [4, 5]. This stress is singular of the form $Kr^{\lambda-1}$, where K is the stress intensity factor and $\lambda < 1$ is a function of the Poisson's ratio [4, 5]. Moreover, K diverges with increasing thickness h of the adhesive as $h^{1-\lambda}$ [6]. This has important practical consequences as it indicates that flaws at corners are especially prone to failure. To understand the connection between the macroscopic stress and molecular scale deformations in polymer adhesives, treatment of systems with open surfaces and corners needs to be done.

To address the above issues, molecular dynamics simulations of a model epoxy system bonding together two solid surfaces with open sides and corners have been performed. The effect of system size on fracture for a model epoxy is examined and connections are made between the molecular scale interfacial dynamics with the system's stress-strain curves. Significant system size dependence of fracture initiation and failure is found. These results have significant implications on the nature of the underlying physical phenomena and in performing comparisons between simulation and experiments on epoxies.

Our previous simulations on coarse-grained, highly crosslinked polymer networks modeling epoxies calculated stress-strain behavior for the network betweeen two parallel plates with periodic boundary conditions on the sides [7–9]. Unexpectedly, very large failure strains were found even though the network was highly crosslinked with very short strand lengths. In experiments on much larger epoxy adhesives, the failure strains are near 0.1 for tensile and are up to about 0.3 for compression [10, 11]. The expectation was that the short strands in an epoxy could only be strained a small amount before bond breaking. The simulations found that the strands have a compact structure that requires a large strain to unfold and does so without stressing the bonds. Consequently, a long plateau regime in the stress-strain curves occurs while the strands are being unfolded and pulled taut. Because the strands are compact, the minimal path length through the network from one surface binding site to the another site on the opposite surface is greater than twice the plate

separation [7]. Only at these large strains, do the strands become sufficiently taut and the stress increase ultimately causing bond breaking and failure. The failure strain in these systems without open sides did not vary signifcantly as a function of system size.

More recently there have been a range of simulations of epoxies [12]. Liu et al. have developed multiscale techniques for curing and construction of the network structure [13]. Atomistic models have been developed and mechanical properties such as the elastic moduli calculated [12, 14–18]. The failure strains for the atomistic simulations of Yang et al. are also large at about 1.0 [17]. Yang and Qu developed a coarse-grained model of an epoxy from atomistic simulations, which like our previous results gives very large failure strains [19].

Local elastic moduli have been calculated for simpler systems and shown to be connected to critical deformations [20–24]. The nucleation of cavities in a uncrosslinked polymer glass under tensile strain has been shown to be where the local elastic moduli are large [23]. Simulations of simpler amorphous solids have found that classical nucleation theory can be used to describe cavitation and similar behavior has been seen in glassy polymers [24]. Given the similarities in the models, the cavitation that occurs in the epoxy tensile simulations during the long plateau of the stress-strain curve should have the same origin [7, 19]. Calculation of the local stress in a corner has not been done for polymers, but the rise of the corner stress with system size on the atomic scale has been seen in simulations of a crystal at very low temperatures [25]. To minimize the fluctuations in the local stress, the simulations had to be performed for crystals and at temperatures close to 0. In polymeric systems, yielding typically occurs limiting the application of linear elasticity, but the concept of large stress in corners is expected to hold and is examined in this work.

The model of highly cross-linked polymer networks is the based on earlier work [7–9]. The polymers are treated as bead-spring molecules. The initial system is a mixture of two molecules. A two bead molecule represents the resin (Bisphenol A) which we label as molecule A. In this work, we introduce a more complicated crosslinker (molecule B) that models the T403 crosslinker as shown in Fig. 1, which has a central bead with three arms of length 2, 1 and 2 beads corresponding to the average lengths of each arm. The three terminal beads on the arms can each form two additional bonds with molecule A, which can form one additional bond for each of its beads. The number of cross-linkers in the system is determined by stoichiometry.

All beads interact through the standard Lennard-Jones (LJ) potential with a cutoff at $2.5d$ [26].

$$U_{LJ}(r) = 4u_0 \left[\left(\frac{d}{r} \right)^{12} - \left(\frac{d}{r} \right)^{6} \right] \tag{1}$$

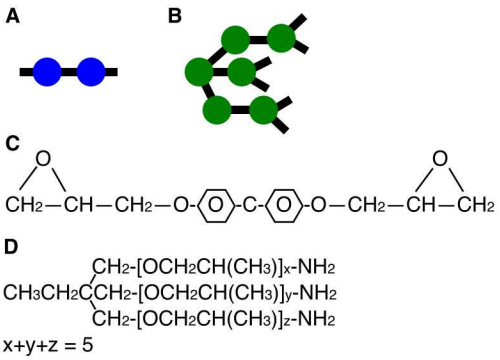

FIG. 1. Schematic of the molecular components of the model epoxy. Molecule A is the coarse-grained represenation of Bisphenol A (molecule C). Molecule B is the coarse-grained representation of the T403 crosslinker (molecule D). The terminal beads have two open bonds on the T403 representing the NH_2 terminal group.

where r is the separation distance, u_0 represents the LJ energy and d represents the size of a bead. The masses of all the beads are taken to be equal, the time unit is τ and all quantities will be in LJ units. The traditional notation of σ and ϵ as the stress and strain, respectively, is used.

The geometry of the system starts with a stoichiometric liquid mixture of the two components between two rigid, solid surfaces. Each solid surface is composed of two fcc (111) layers perpendicular to the z-direction with a near neighbor spacing in the layer of $1.204d$. Periodic boundary conditions are imposed in the y-direction; the size of the simulation cell in this direction is $28d$ for all systems. The width in the x-direction w and the separation of the surfaces h varies with the system (see Table I). The h/w ratio is about 10 in all cases so that the central region should not be influenced by the sides.

The polymeric system is composed initially of a stoichiometric mixture of the two molecules between two solid surfaces. The starting liquid extends to about $5d$ from the open ends of the surfaces. In the x-direction the system is open except during equilibration of the liquid mixture of the two components, when a wall potential is used to confine the liquid. After equilibration, the wall potential is removed and bonding to the surfaces and crosslinking of the liquid occurs as in previous simulations [8]. The crosslinking simulation time is long enough such that at least 95% of the possible bonds are formed. Crosslinking is performed slightly above the glass transition temperature. The systems is then cooled to $0.3u_0$ (below the glass transition temperature) and a simulation run until the thickness of the system reaches a steady state under a load $(0.1u_0/d^3)$ on the top surface mimicking atmospheric pressure. Tensile simulations are performed by pulling the

TABLE I. Systems

index	N	h	w
1	513600	40.4	417.1
2	1975200	76.1	834.2
3	7747200	149.0	1668.3
4	17316000	222.3	2502.5
5	30681600	295.0	3366.6

top surface at a constant velocity of 0.001 d/τ. For system 2, the pull velocity was verified to be slow enough that there are not resolvable differences in the stress-strain curves compared to $10^{-4} d/\tau$.

The stress-strain behavior is shown in Fig. 2 for the system sizes given in Table I. The data has been boxcar smoothed. A clear dependence on h occurs in the stress-strain behavior at large strain,

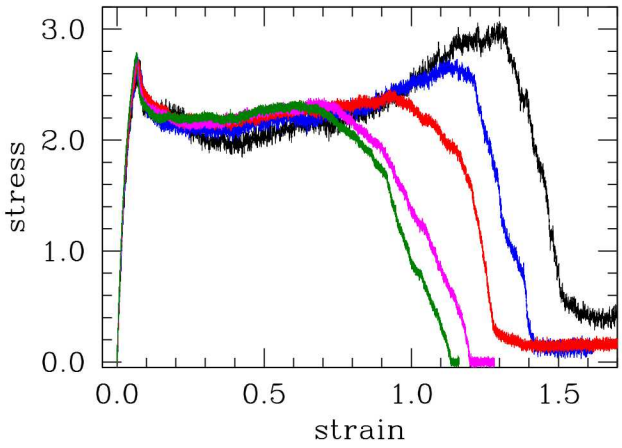

FIG. 2. The stress-strain curves as a function of system size for systems 1-5. Colors are black, blue, red, magenta and green for systems 1 to 5, respectively.

but the low strain behavior has similar behavior. The yield stress peak is identical for all systems. For sufficiently large systems where the surfaces (including sides) are not affecting the bulk, the yield behavior should be independent of size, since the dynamics of the beads at small strains is local. The yield stress is 2.85 u_0/d^3, and the yield strain ϵ_y is 0.073. For a wide range of $\epsilon > \epsilon_y$, the behavior is similar for all systems with the larger systems having smaller fluctuations. In this regime, there is a long plateau in the stress at about 2.2 u_0/d^3. From previous work [7, 8], this

plateau region is where the strands are being straightened by the tensile stress and very few of the the bonds are being strained. Because the tensile pull is increasing the volume, voids are forming on the molecular scale (see Fig. 3). At larger ε, the stress rises because bonds are being stretched. At this point, a distinct size dependent behavior does occur. The rise in the stress is rather small in the largest systems remaining well below σ_y, while the smallest system has a maximum stress greater than σ_y. The failure strain ε_f is calculated as the strain value at which the stress is half the maximum. Clearly, the failure strain ε_f decreases as a function of system size.

The critical difference from the present work and past fracture simulations is the explicit treatment of the open sides and corners. The mode of fracture initiation is distinct due to the open boundary. Examination of images of the system as a function of strain show that in all systems, a crack forms in one (or two) of the corners as shown in Fig. 3 (see also the Supplement for images of all systems). The strain at which the crack appears ε_c is determined from visual inspection of the images of the dynamics. Fig. 4 shows the dependence on h of ε_c, ε_f and ε_p, the strain at the peak stress. Note that the ε_p are the same as ε_c given the uncertainty in both values, except for the smallest system. This equality is to be expected, since once the crack starts the stress also begins to be relieved and decreases.

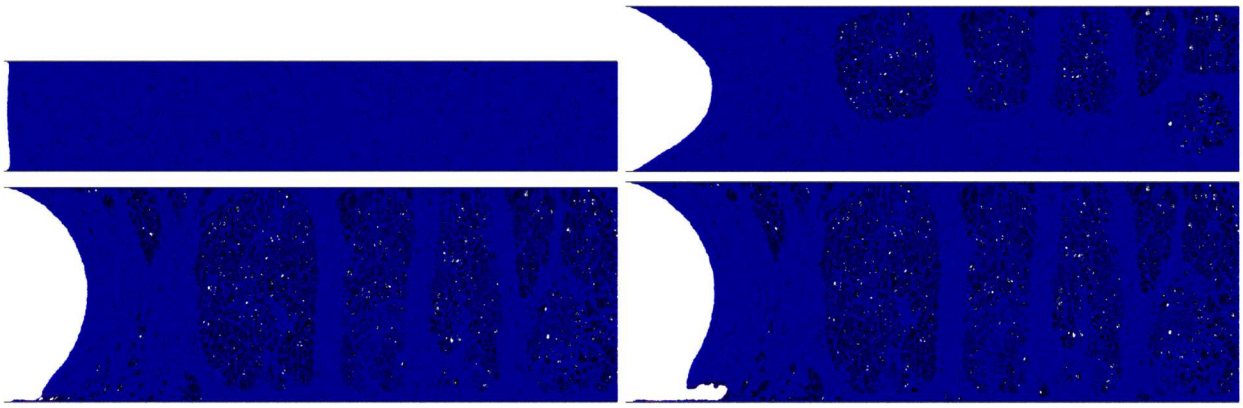

FIG. 3. Images of left half of system 3 at various ε showing crack formation at corner and contraction of side. Void formation is also visible for $\varepsilon > 0$. From top to bottom $\varepsilon = 0$, 0.50, 0.95 and 1.00.

The extrapolations in Fig. 4 have significant implications. For large h the extrapolation of ε_c implies cracks will form at zero strain for h near $550d$ [27]. This extrapolation comes from linear least squares fits to ε_f and ε_c. The extrapolation to $\varepsilon_f \to 0$ occurs near $h = 800d$. If we use d =1 nm as an estimate of the bead size, then all these thicknesses are below a micron. These results imply that a major source of the difference between simulations of highly crosslinked polymer and

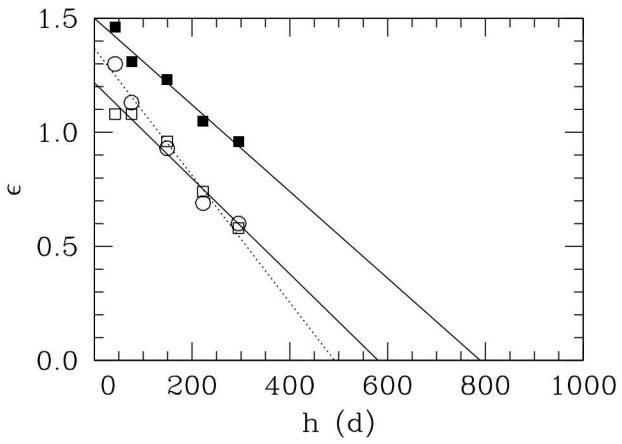

FIG. 4. The failure (solid squares), (second) maximum peak stress (open circles) and crack initiation (open squares) strains as a function of the adhesive thickness (h). The lines are separate least squares fits to each data set, with the dotted line for the ε_p data and the solid lines for the other two.

experiments is the geometry and system size. The data implies that the failure strains in simulations for system sizes typical in experiments could easily be in the range seen in experiments. Directly comparing to experiments on adhesives on the submicron scale is limited by the sparse experimental data available on such thin systems due to inherent measurement challenges [28].

An intriguing point is that this h-dependence implies the existence of a new length scale. The extrapolations of ε_c and ε_f are expected to break down, as new physical phenomena ought to occur as ε_c approaches ε_y let alone 0. Thus, there must be a thickness h^*, where the decreasing ε_c stops or changes. This h^* will be indicative a structural length scale that is significant in understanding large scale deformation in highly crosslinked polymer networks. Unfortunately, resolving this issure requires larger simulations than we can do.

In previous work on systems without open sides, we found the failure strain was correlated with the minimal paths in the network from bottom surface to the top surface, and this connection was the determining factor of the the large failure strains [7]. In the present systems, there is a difference in behavior between the sides and the center. In the center of the system, the behavior is similar to the early simulations, as the structure of the strands is similar to previous works. The minimal path lengths in the center written as a strain, $\varepsilon_{\rm mp} \equiv P_{\rm min}/h - 1$ are in the range 1.30 to 1.33. The minimal paths near the edges are slightly shorter ($\varepsilon_{\rm mp} \simeq 1.26$), since the paths do not have complete freedom of direction that exists at the center, but this is not a source of the h dependence.

As Fig. 3 shows the shape of the sides changes with strain as the cohesive forces try to maintain

the equilibrium density by contracting the polymer network from the sides, i.e. necking. The shape at the corners becomes an acute wedge that extends over a relatively long length as the side contract in. The minimal paths near the sides are stretched along a curved path, which is longer than the straight path for the central minimal paths. The paths near the sides are thus much more stretched at a given strain than paths in the center are. The minimal paths at the sides will become taut at lower strains than at the center because of the curved paths at the sides. The length of side as a function of ε was calculated (for a range of strains a parabola is a good fit to the shape). The dependence of the side shape and length as a function of strain has an interesting connection with ε_{mp} (see Supp. Fig. S3). For $\varepsilon \lesssim 0.55$ the amount of inward necking increases monotonically and is independent of the h. At larger ε the amount of necking decreases. This transition occurs when the side length approaches the minimal path length of the sides. Thus, at the sides there is a much larger strain than in the middle of the system and it saturates at ε_{mp}. Once the strain along the sides approaches close to the ε_{mp} the minimal paths along the side are almost taut and the degree of necking reverses to keep the side contour length constant. However, neither ε_f nor ε_c are correlated with this transition which is constant with respect to h.

In order to get a better understanding of the fracture dynamics, the location of individual bond breaking in the systems as a function of ε was examined. Bond breaking starts well below ε_c in two regions: in the voids and at the sides (see Fig. S9). Within the voids, the bond breaking is sporadic spatially and does not accumulate into a crack. However at the sides and particularly the corners, the number of broken bonds increases with strain and does result in cracks. As a function of h, the total number of broken bonds is monotonically increasing at $\varepsilon = 0.50$, which is below ε_c for all h. A concentration of bond breaking in the corners implies there is a concentration of stress there.

The local stress was calculated using the local virial with voronoi volumes [29]. However, calculating the local stress encounters various limitations. The fluctuations in stress are large even when dealing with the whole system or surface. At the level of a smaller grid, the fluctuations will be even larger. We calculated the stress binned into bins of size $4d \times 4d$ in the xz-plane. At $\varepsilon = 0$, the stress is effectively uniform with no indication of high stress in the corners. However, as the strain increases, clear stress concentration in the corners is exhibited in σ_{xx} as shown in Fig. 5. Large values of σ_{zz} occur not in the corners but in the middle of the sides. These high stresses and their direction correlate with necking geometry and bond breaking discussed above. The contraction of the sides results in a wedge shaped geometry in the corners, with the bonds

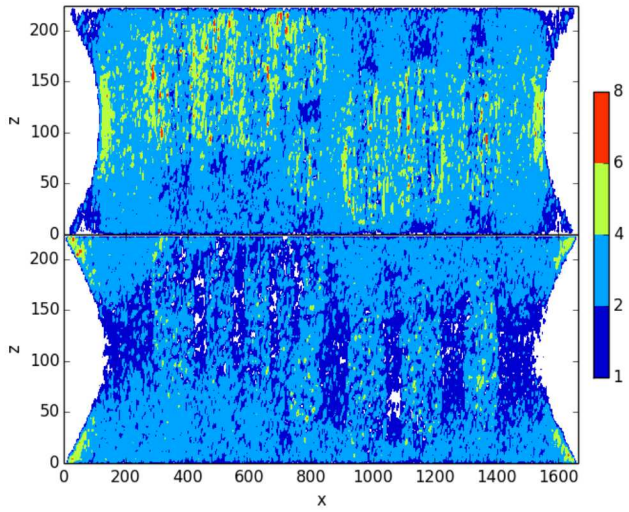

FIG. 5. The local stresses σ_{zz} (top) and σ_{xx} (bottom) for system 3 at $\varepsilon = 0.50$.

being primarily strained in the x-direction. Thus the corners have large σ_{xx}. The network at the middle of the sides is also strained by the tension, but at this location the strain is the z-direction. Thus the middle of the sides have large σ_{zz}. We note that within the system the nanovoiding also give pockets of large σ_{zz} in the interior.

These tensile simulations of a coarse-grained highly crosslinked polymer system with open sides have produced several important results. The failure stain decreases substantially as the system size is increased, showing that system size and boundary conditions are critical. Extrapolating this size effect implies that systems with thickness of less than a micron will have failure strains similar to observed in experiments. Thus, a major source of the large difference in failure strains between simulation and experiment has been identified. Moreover, the results imply the existence of a crossover, where the failure strain stops decreasing with system size, and this crossover corresponds to an important length scale in the polymer adhesive system that has not be characterized. As in experiments the open sides result in the stresses that cause bond breaking to localize predominantly in the corners. Crack initiation is found to occur in the corners as would be expected from linear elastic fracture mechanics, although with such large strains the system is not in the linear regime. Future simulations will address larger systems to observe the transition in $\varepsilon_f(h)$ and to determine the structural feature(s) that determine the transition.

Supported by the Laboratory Directed Research and Development program at Sandia National Laboratories, a multi-program laboratory managed and operated by Sandia Corporation, a wholly owned subsidiary of Lockheed Martin Corporation, for the U.S. Department of Energy's National

Nuclear Security Administration under contract DE-AC04-94AL85000.

[1] A. J. Kinloch, *Adhesion and Adhesives* (Chapman and Hall, New York, 1987).

[2] K. Kendall, Science **263**, 1720 (1994).

[3] C. Gay and L. Leibler, Phys. Rev. Lett. **82**, 936 (1999).

[4] M. Williams, Journal of Applied Mechanics **19**, 526 (1952).

[5] S. Timoshenko and J. Goodie, *Theory of Elasticity* (McGraw-Hill Book Company, New York, 1970).

[6] E. R. Jr., Eng. Fracture Mech. **36**, 575 (1990).

[7] M. J. Stevens, Macromolecules **34**, 1411 (2001).

[8] M. J. Stevens, Macromolecules **34**, 2710 (2001).

[9] M. Tsige and M. J. Stevens, Macromolecules **37**, 630 (2004).

[10] R. J. Morgan, F.-M. Kong, and C. M. Walkup, Polymer **25**, 375 (1984).

[11] W. Chen and B. Zhou, Mechanics of Time-Dependent Materials **2**, 103 (1998).

[12] C. Li and A. Strachan, J. Polymer Science, B **53**, 103 (2015).

[13] H. Liu, M. Li, Z. Lu, Z. Zhang, C. Sun, and T. Cui, Macromolecules **44**, 8650 (2011).

[14] C. Wu and W. Xu, Polymer **47**, 6004 (2006).

[15] C. Wu and W. Xu, Polymer **48**, 5802 (2007).

[16] V. Varshney, S. S. Patnaik, A. K. Roy, and B. L. Farmer, Macromolecules **41**, 6837 (2008).

[17] S. Yang, F. Gao, and J. Qu, Polymer **54**, 5064 (2013).

[18] C. Li, G. A. Medvedev, E. Lee, J. Kim, J. M. Caruthers, and A. Strachan, Polymer **53**, 4222 (2012).

[19] S. Yang and J. Qu, Phys. Rev. E **90**, 012601 (2014).

[20] J. Rottler, J.Physics: Condensed Matter **21**, 463101 (2009).

[21] I. Chikina and C. Gay, Phys. Rev. Lett. **85**, 4546 (2000).

[22] K. Yoshimoto, T. S. Jain, K. V. Workum, P. F. Nealey, and J. J. de Pablo, Phys. Rev. Lett. **93**, 175501 (2004).

[23] A. Makke, M. Perez, J. Rottler, O. Lame, and J.-L. Barrat, Macromolecular Theory and Simulations **20**, 826 (2011).

[24] P. Guan, S. Lu, M. J. B. Spector, P. K. Valavala, and M. L. Falk, Phys. Rev. Lett. **110**, 185502 (2013).

[25] O. Vafek and M. Robbins, Phyical Review B **60**, 12002 (1999).

[26] K. Kremer and G. Grest, "Entanglement effects in polymer melts and networks," in *Monte Carlo and*

Molecular Dynamics Simulations in Polymer Science, edited by K. Binder (Oxford, New York, 1995) Chap. 4, pp. 194–271.

[27] Simulations of larger h are not presently possible with our resources. The system 5 simulations already take about 2 months of CPU time.

[28] D. Lau, K. Broderick, M. J. Buehler, and O. Büyüköztürk, Proceedings of the National Academy of Sciences **111**, 11990 (2014).

[29] D. MacNeill and J. Rottler, Phys. Rev. E **81**, 011804 (2010).

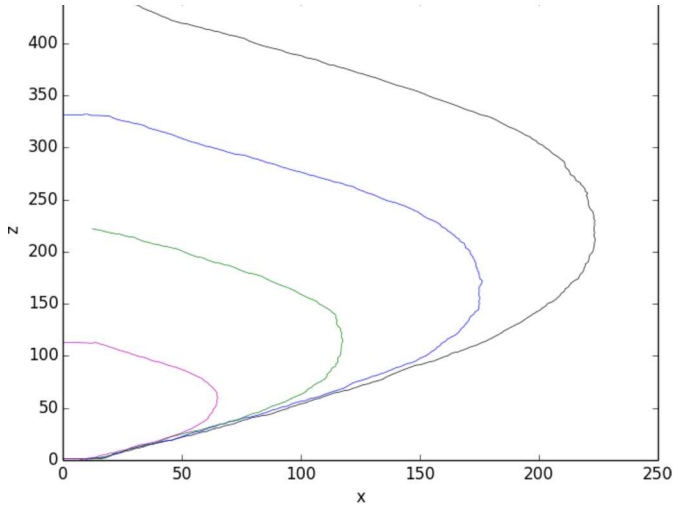

FIG. S1. The left side density contour at 0.5 σ^{-3} as a function of h at $\varepsilon = 0.5$.

SUPPLEMENT

The shape of the neck region as a function of system size can be well described by the density contours at the sides. In Fig. S1 the contours of the left side at $\varepsilon = 0.5$ is shown for all five systems. The shape of the corner is shown to be similar for all cases. More specifically, the slope of the wedge shape is identical. The extent of the inward necking increases with h.

At intermediate values of the strain, this side shape can be well fit by a parabola as shown in Fig. S2. In these cases, the length of the side can be quite accurately calculated. In cases where the shape deviates from a parabola, the length has been determined from the two bounding parabolic fits. The uncertainty that results in this method is small enough not to impact the points made in the main text.

The dependence of the side shape as a function of strain for system 3 is given in Fig. S3. The main features are that the inward extent increases with strain to about $\varepsilon = 0.60$, which is shown in green. By this strain, the length of the side has reached the minimal path length of the network at the sides. At larger strains, the inward extent *decreases* so that the total side length remains about constant. For system 3 this behavior continues to much larger strains before a crack forms in the corner.

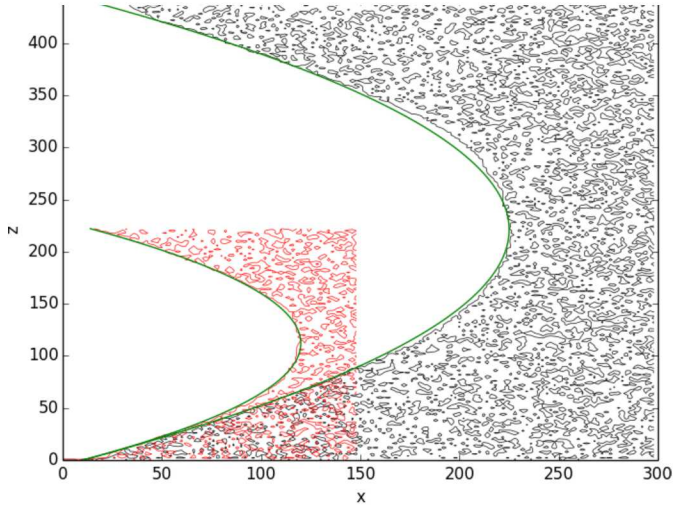

FIG. S2. The left side density contour at 1.0 σ^{-3} for systems 3 and 5 at $\varepsilon = 0.5$ showing parabolic fits (green) to the sides.

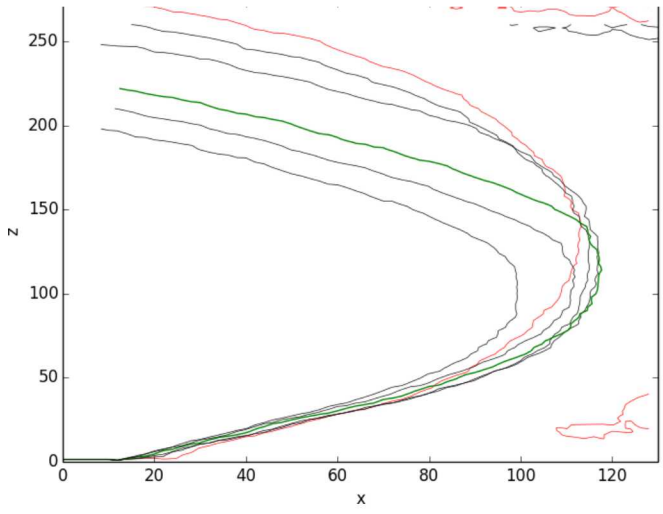

FIG. S3. Strain dependence of the left side for system 3. $\varepsilon = 0.33, 0.415, 0.50, 0.60(green), 0.75$ and 0.83 (red). Some contours away from the side show up at the two largest strains due to void formation at these large strains.

Figures S4-S8 show images of all the systems at different strains. The dark regions are where cavities have formed.

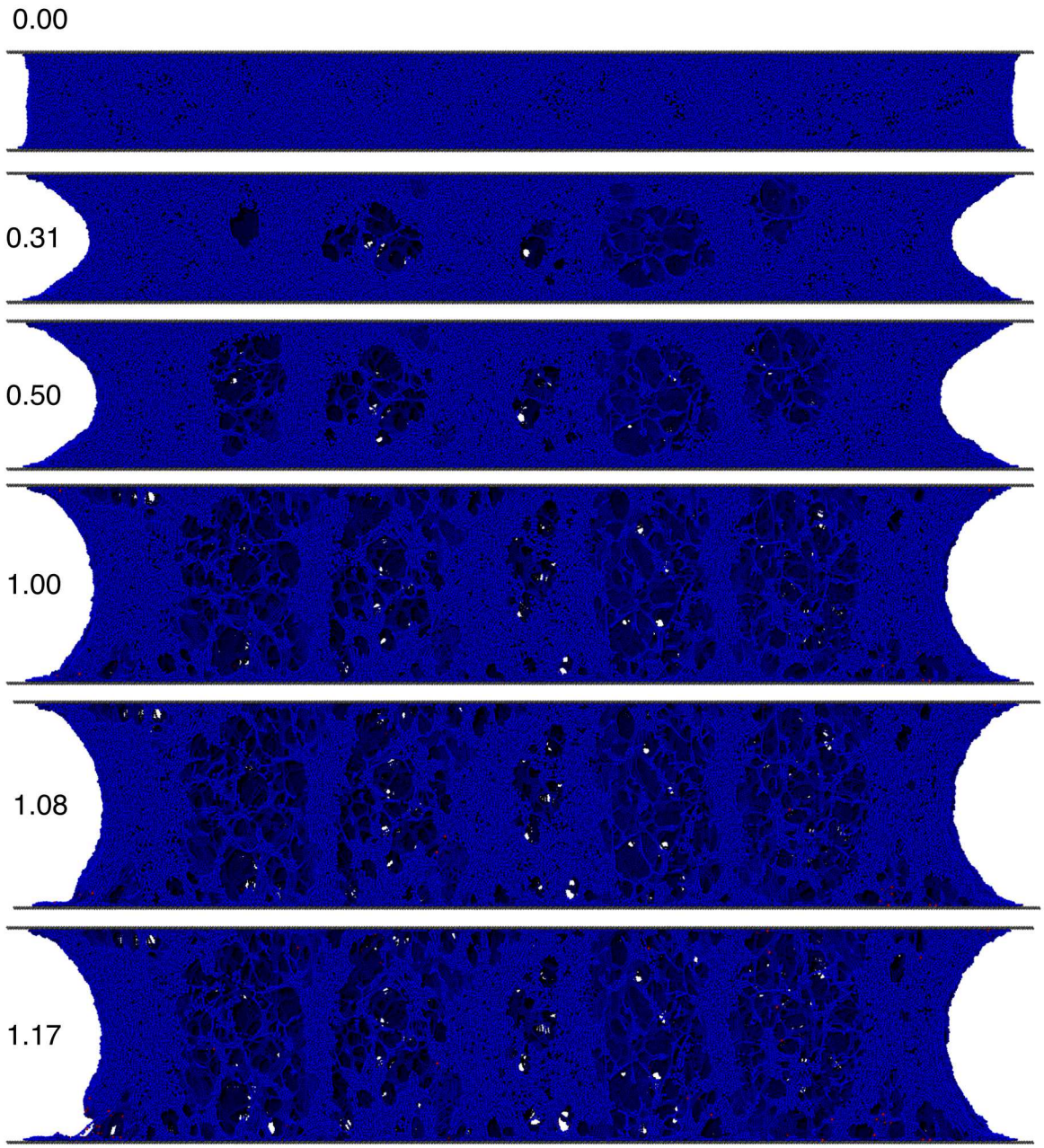

FIG. S4. Images of system 1 at various ϵ showing crack formation at corner and contraction of side.

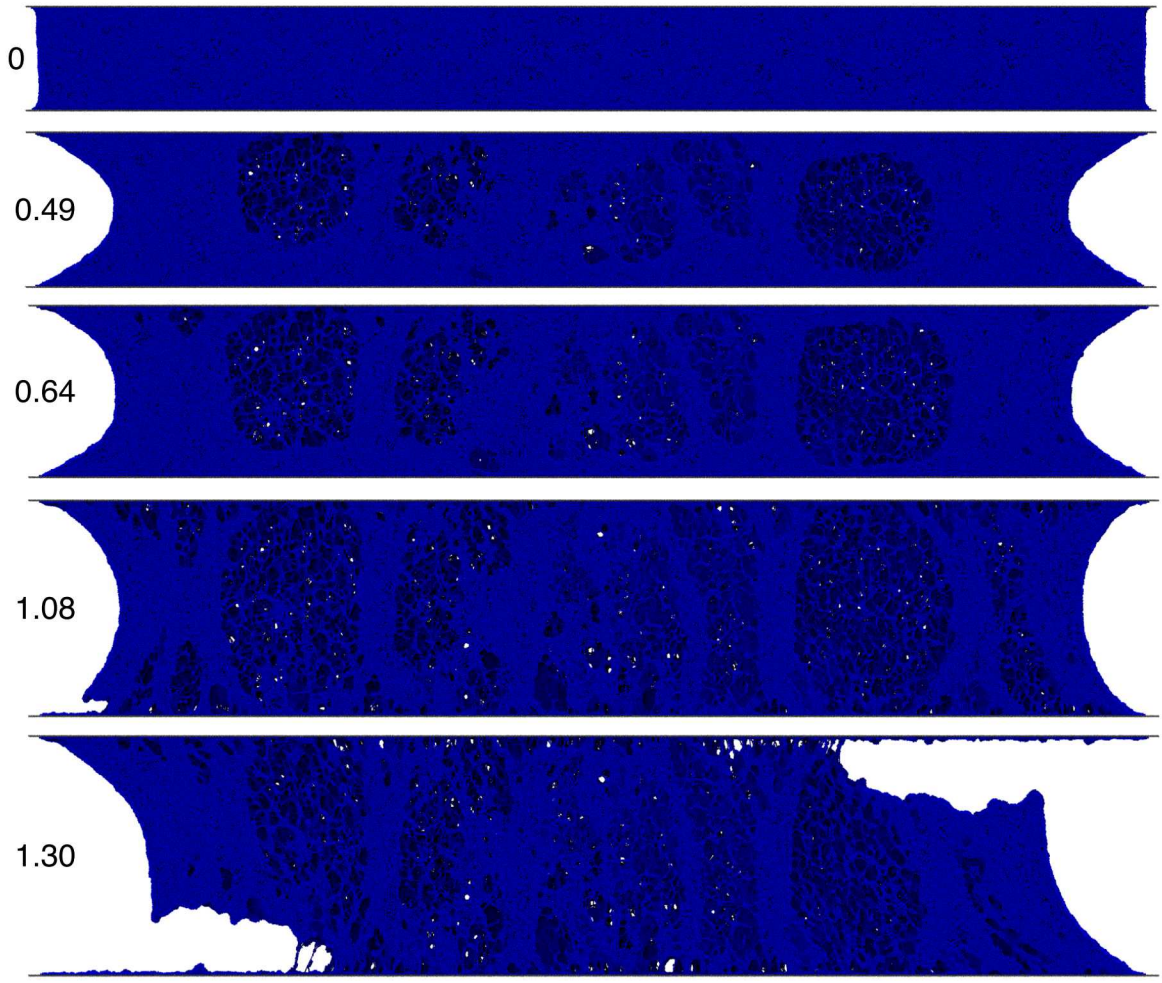

FIG. S5. Images of system 2 at various ϵ showing crack formation at corner and contraction of side.

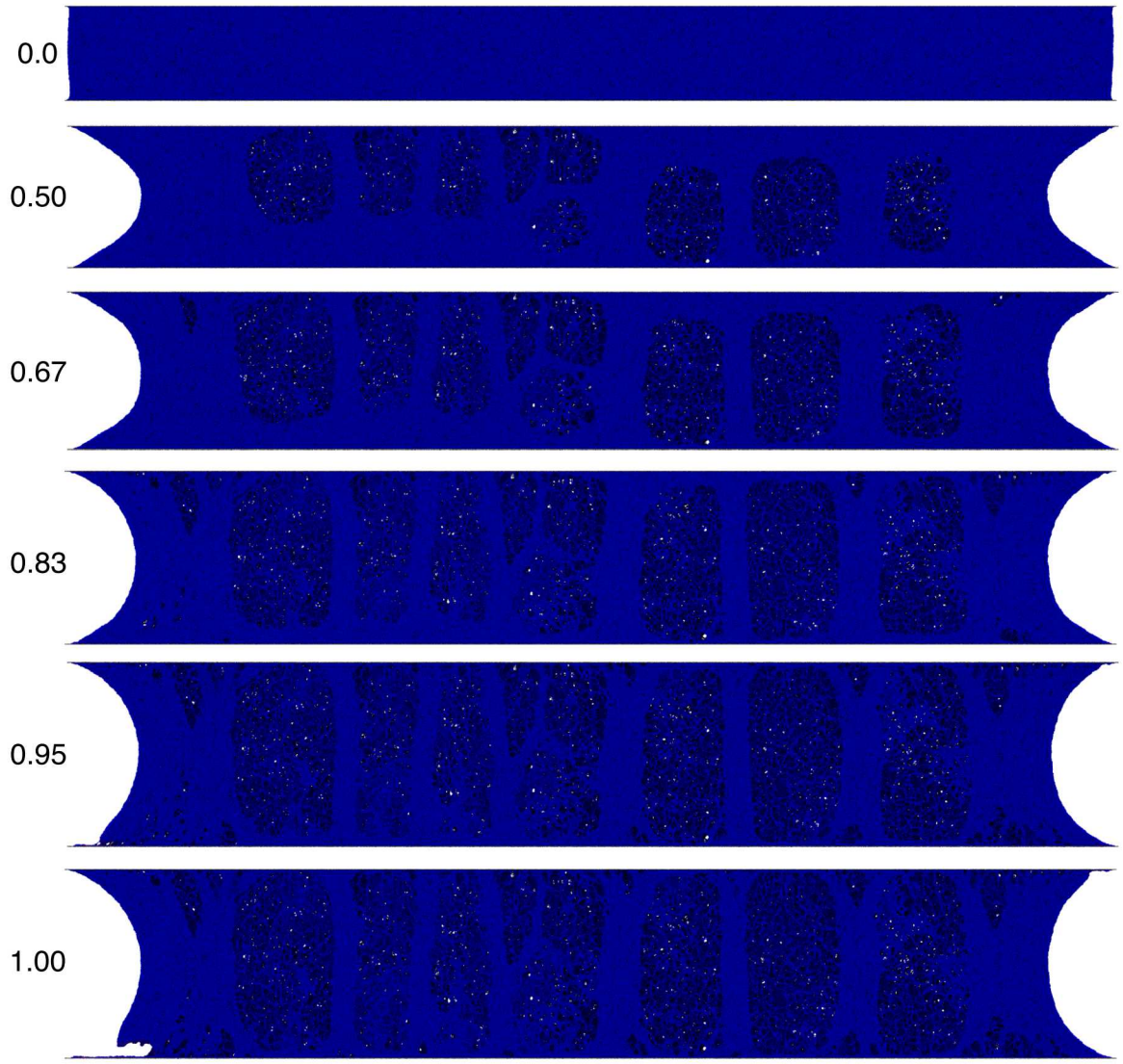

FIG. S6. Images of system 3 at various ϵ showing crack formation at corner and contraction of side.

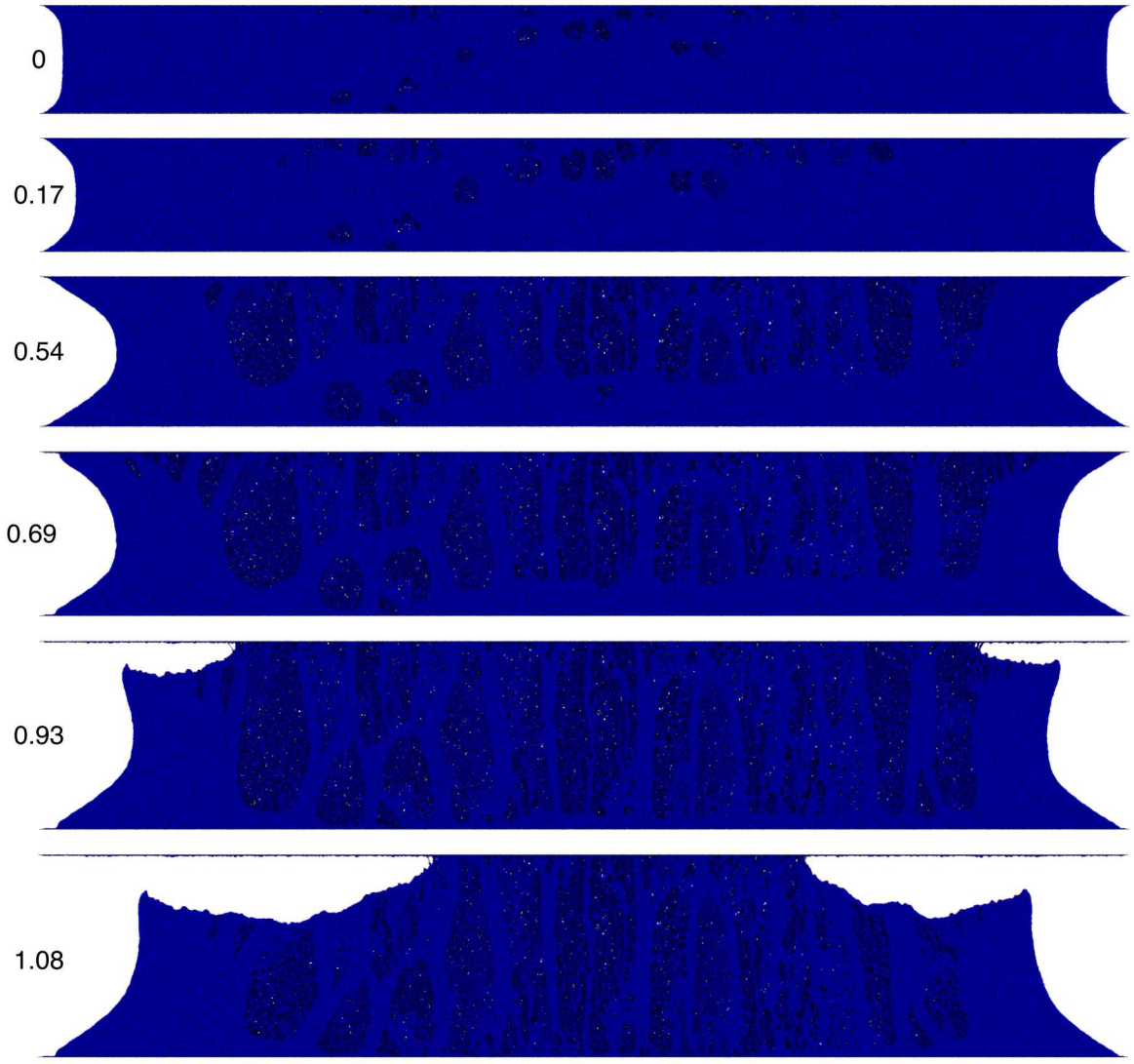

FIG. S7. Images of system 4 at various ϵ showing crack formation at corner and contraction of side.

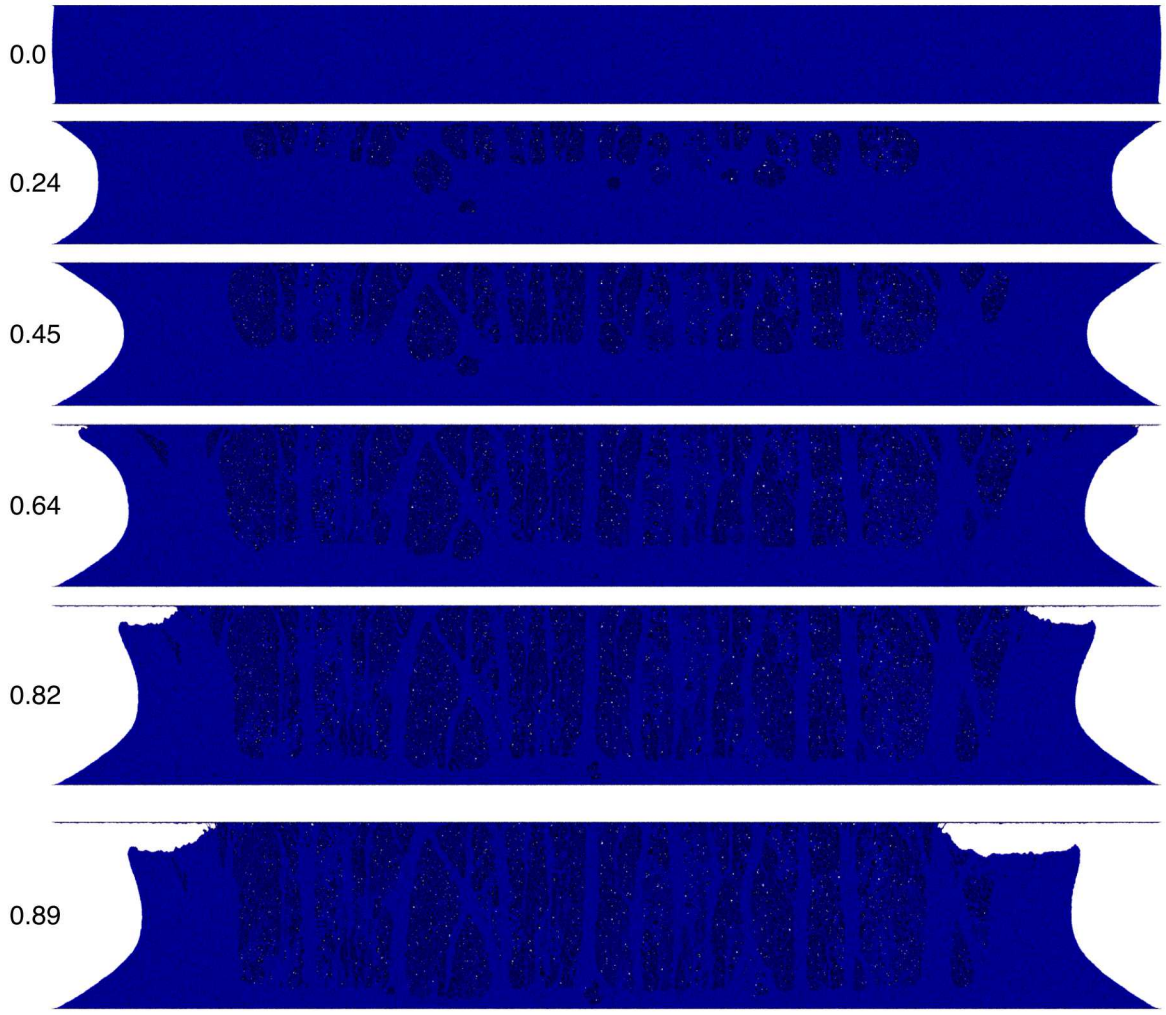

FIG. S8. Images of system 5 at various ϵ showing crack formation at corner and contraction of side.

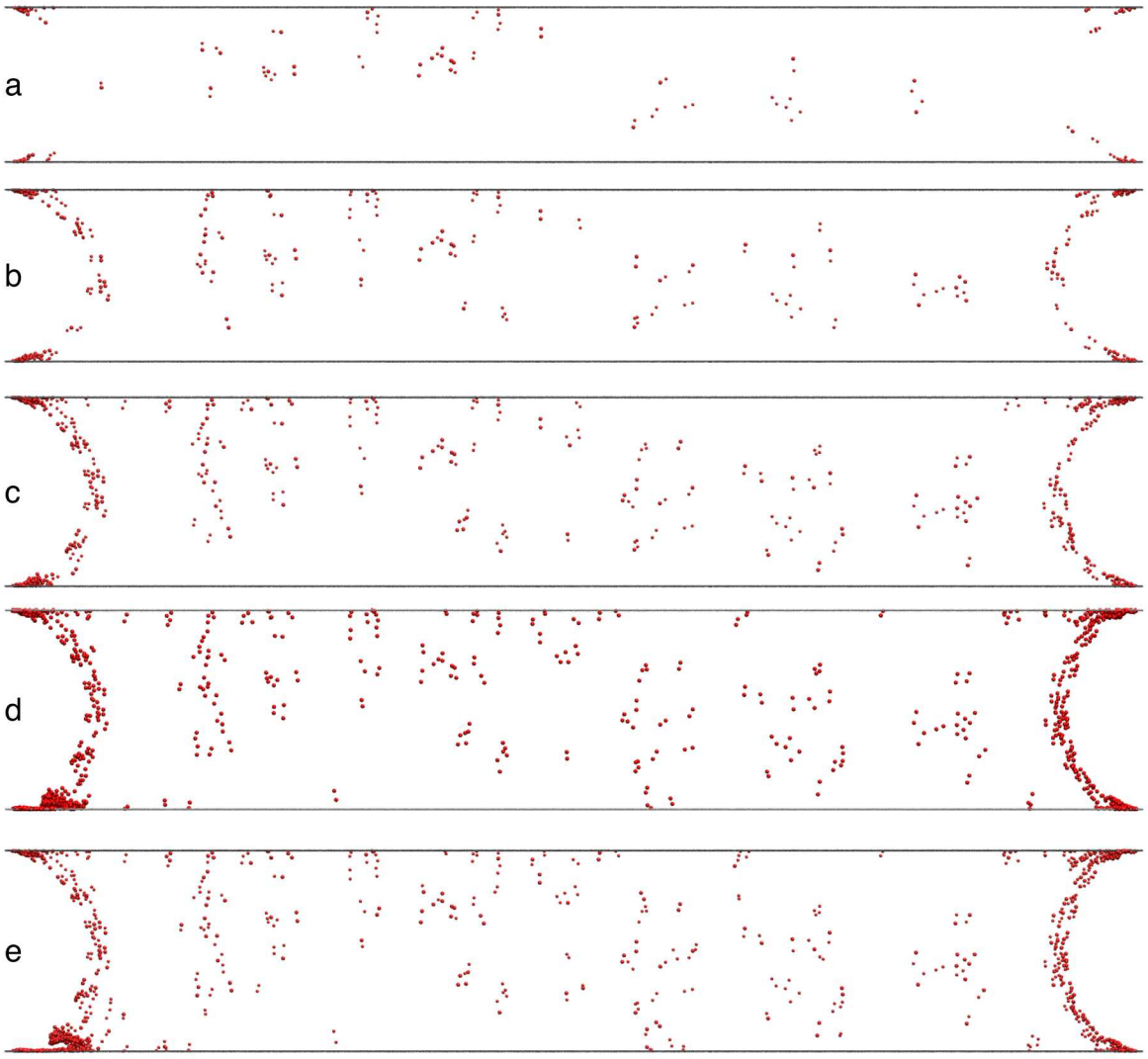

FIG. S9. Images showing broken bonds (red) and surfaces (gray) as a function of strain for system 3. ϵ = a) 0.50 b) 0.67 c) 0.83 d) 0.95 e) 1.00.

The location of broken bonds as a function of strain for system 3 are shown in Fig. **??**. Bond breaking does start well before ε_c, but initially it is mostly isolated bonds. An accumulation of bond breaking in the corners and along the sides occurs as the strain approaches ε_c, and finally a crack forms once sufficient bond breaking in the corner occurs.